Imploding Z-Pinch Plasmas Formed From a Carbon Fiber

Daniel Klir, Pavel Kubes, and Jozef Kravarik

***Abstract*—Z-pinch experiments, which are formed from a 15-μm diameter carbon fiber in a vacuum, were conducted using a simple capacitor bank. After the breakdown, a low-density coronal plasma was formed while the fiber diameter remained almost unchanged. This low-density corona (ion density of about 10^{16} cm^{-3}) was carrying almost all the current of the order of 10 kA. When the current had built up, i.e., after about 150 ns, the implosion of the corona onto the central fiber occurred. The implosion velocity approached the value of $2 \cdot 10^5$ m/s. When the imploded corona had reached the fiber, the dip in dI/dt, a voltage peak up to 10 kV and an extreme-ultraviolet (XUV) pulse of a 10–30-ns width were observed. XUV radiation was emitted from several bright spots, which corresponded to the interaction of $m = 0$ instability necks with the dense core. The electron temperature and density were approximately 80 eV and 10^{19} cm^{-3}, respectively. Although the presence of a fiber did not significantly suppress MHD instabilities, they were not disruptive. After the fiber ablation, i.e., after 500 ns, the material evaporated from the electrodes started to play a dominant role. When MHD instabilities had developed in the imploding plasma column, XUV, soft X-ray, and hard X-ray pulses were emitted from several bright spots, particularly near the anode. At that time, the voltage peak of up to 30 kV was detected. The measurement of voltage and current enabled the determination of a plasma resistance and the energetics of the Z-pinch.**

***Index Terms*—Bright spots, carbon, Extreme ultraviolet (XUV) radiation, fiber Z-pinch, implosion, plasma diagnostics.**

I. Introduction

THE HIGH-DENSITY Z-pinches, which are formed from dielectric fibers in a vacuum, were investigated in the 1980s and 1990s in connection with the research of controlled thermonuclear fusion and radiative collapse (see [1]–[13] and references therein). The notion was to heat and ionize the fiber from a frozen deuterium and to confine the high-density and high-temperature plasma column within a small diameter. Since the development of instabilities and global expansion of a pinch column were observed from the very beginning of the discharge, the idea of the fiber Z-pinch as a fusion reactor was abandoned.

The fibers from the carbon were also tried in these fiber Z-pinch experiments, because their discharge behavior was roughly the same as the frozen deuterium ones (see [7] and [11]); at the same time, they were easily available and could be handled much easier. Most of the experiments utilized high-voltage pulsed-power systems with a fast current rise time, so as to prevent the early expansion of a plasma column [14]. However, several experiments with a carbon fiber were also performed on a simple capacitor bank. In the experiment carried out at the Czech Technical University (CTU), short ($\approx$ 20 ns) extreme ultraviolet (XUV) pulses were observed [15]. This result led to the idea of using a carbon-fiber Z-pinch as an XUV laser; however, the origin of the short XUV pulses was not studied in greater detail. Another experiment with a microsecond-long capacitive discharge (in this case, at Ruhr Universität, Bochum, at atmospheric pressure) was performed in order to measure the electrical conductivity of the nonideal carbon plasmas [16].

In this paper, we aim at presenting the most important results from a carbon-fiber Z-pinch driven by a low-voltage capacitive discharge. The primary objective of our research is the description of the carbon-fiber Z-pinch dynamics. We believe that our findings help us to get a deeper insight into the processes, which are taking place in Z-pinches (breakdown physics, implosion of a low-density plasma, carbon-fiber ablation, dynamics of bright spots, etc.). We try to take the advantage of a small-scale experiment, which could be easily modified, and in some cases, better diagnosed, while it remains interesting from the physical point of view. We put an emphasis on comprehensive diagnostics, and thus, the higher number of diagnostic methods is applied in order to verify the obtained results.

II. Apparatus and Diagnostics

A. Experimental Setup

During the past four years, more than 500 shots have been performed on a small Z-pinch. The generator employed to drive recent experiments, consisted of one capacitor with the capacitance of $C_0 = 3$ μF. In the case of a 20-kV charging voltage, the current was peaking at 80 kA with the quarter period of about 850 ns. The circuit inductance of $L_0 = 100$ nH and the resistance of $R_0 = 25$ mΩ were estimated from the damped oscillation of a short circuit.

The experimental chamber of a 6.5-cm height and 8-cm diameter was made of a stainless steel and was evacuated to a pressure of 10^{-2} Pa. Carbon fibers of 15-μm diameter and 7–9-mm length were mounted between the live anode and the cathode, which were isolated from each other by an alkaline polyamide spacer. As we wanted to distinguish general features of the experiment from specific ones, we performed a few experimental series with electrodes from different materials

Manuscript received December 9, 2005; revised February 28, 2006. This work was supported in part by Research Programs Ministry of Education of the Czech Republic (MSMT) under Grants 1P04LA235, 1P05ME761, and LC 528, and in part by Grant Agency of the Czech Republic (GACR) under Grant 202-03-HI62.

The authors are with the Faculty of Electrical Engineering, Czech Technical University, 166 27 Prague, Czech Republic (e-mail: klird1@fel.cvut.cz).

Digital Object Identifier 10.1109/TPS.2006.878614

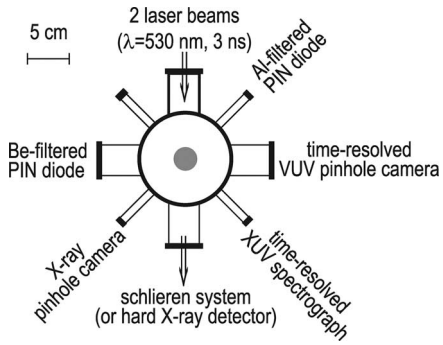

Fig. 1. Schematic diagram of the diagnostic setup, end on view.

(copper, steel, brass, and bronze) and of different shape (flat, conical, etc.).

B. Diagnostics

Fig. 1 shows that the radiation emitted from the plasma was recorded with two filtered p-i-n diodes, a hard X-ray detector (HAMAMATSU H1949-51 PMT and Bicron BCF-12 scintillating fiber), a gated XUV spectrograph, a gated vacuum ultraviolet (VUV) pinhole camera, and with a differentially filtered time-integrated X-ray pinhole camera. Two p-i-n diodes and the time-integrated pinhole camera were differentially filtered with a Be filter (15 μm) and an Al foil (0.8 μm or 1.5 μm). The temporal resolution of the gated spectrometer and the pinhole camera was carried out with two four-frame microchannel plate (MCP) detectors with the exposure time of 2 ns and the interframe time of 10 ns.

The visualization of the electron-density gradient was enabled by the laser probing (schlieren method). The beam of a frequency-doubled Nd:YAG laser [530-nm wavelength 3-ns pulsewidth] full-width at half maximum (FWHM) was split into two beams, and one of them was delayed by 10 ns with respect to the other. In order to take these two schlieren photographs simultaneously with two pinhole images and two gated XUV spectra, the laser-beam pass length was adjusted. The sensitivity of the schlieren setup was $(5-15)\cdot 10^{18}$ cm$^{-3} < \int \nabla_{\perp} n_{\mathrm{e}}\, dl < 4\cdot 10^{20}$ cm^{-3}. The spatial resolution of the schlieren system was less than 30 μm.

With regard to detectors, charged-coupled-devices (CCD) cameras were employed as recording media for all the time-resolved diagnostics. The X-ray film Kodak Industrex CX was used in the case of time-integrated X-ray pinhole.

The electrical characteristics of the Z-pinch discharge were monitored by the P6015 Tektronix HV probe and dI/dt probe, i.e., Rogowski coil. The plasma spread over a significant part of the chamber, at around 400 ns after the breakdown, and thus, the current flowing through the Rogowski coil was reduced. That was the reason why the dI/dt probe gave inaccurate results after 400 ns, and we gained more information about the electrical characteristics from the voltage waveform.

III. Experimental Results

Typical waveforms recorded in our Z-pinch are shown in Fig. 2. In this particular shot, the Z-pinch discharge was initiated from a carbon fiber with the charging voltage of 20 kV and with the conical electrodes made of bronze. The interesting and characteristic features that we observed were short pulses detected with filtered p-i-n diodes. These pulses were emitted regardless of what charging voltage, material of electrodes, and the diameter of a carbon fiber we tried. Therefore in the following, we would like to elucidate the origin of these pulses and describe what happens in each stage of the discharge.

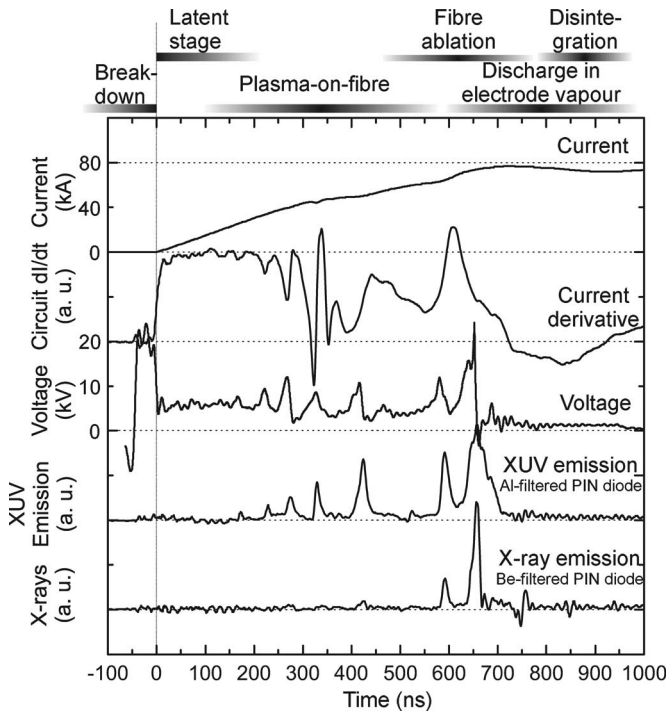

Fig. 2. Waveforms of the current, current derivative, voltage, and p-i-n diode signals recorded in discharge no. 050128-1.

A. Breakdown

It is well known that the breakdown phase is very much influenced by initial physical properties of a Z-pinch load. In the case of a carbon fiber, the characteristic initial property of the material is its high resistivity. The measured resistance of a 1-cm long, 15-μm diameter fiber was about 7 kΩ at room temperature. It is so high resistance that a carbon fiber behaves almost as an insulator, and it takes some time for the breakdown to occur. The voltage does not collapse until a lower resistance and low-density plasma is formed from a desorbed gases/vapors around a fiber. The delay between the rise of the voltage and the current derivative can be seen in Fig. 2. In the case of a 20-kV charging voltage, we obtained the delay of 50 $\pm$ 10 ns.

However, the resistance is not the only fact that influences the electrical breakdown. Sarkisov *et al.* reported the significant effect of the radial electric field and its polarity [17] (in our case $E_{\mathrm{r}} > 0$). This radial electric field caused the breakdown to start at the cathode where the potential barrier for electronic emission was lowest. As a result, the deposited energy at the cathode was lower because the direct heating was prevented by a shunted current. We measured that the Joule heat produced before the voltage collapse was about 20 mJ. It is much lower than the energy required for atomization of a 15-μm carbon

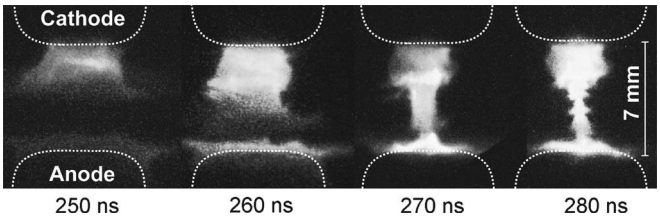

Fig. 3. VUV pinhole images detected in shot no. 030828-1. The last image corresponded to the peak of the 20-ns XUV pulse.

fiber, which is about 200 mJ. Moreover, the energy of 20 mJ was deposited rather to an ambient vapor than to a fiber. Hence, the diameter of a carbon fiber remained almost unchanged after the breakdown.

B. Latent Phase

The "latent phase" of the discharge represents the time after the breakdown and before the appearance of the XUV pulses, i.e., from 0 to about 150 ns. During this phase, the plasma emitted a small amount of radiation, and the electron density was too low to be detected by the schlieren system. Most of the VUV radiation came from the vicinity of the electrodes, especially the anode. This observation agrees with the XUV spectra where the spectral lines of oxygen and higher-Z ions (Cu, Sn, Zn, etc.) were identified. The electron temperature estimated from Li- and Be-like oxygen ions was 15–25 eV.

According to theoretical predictions and experimental observations (e.g., [10]), we can assume that during the latent phase, a low-density plasma expanded to a radius of several millimeters.

C. Plasma on Fiber

The phase between 100 and 500 ns was characterized by short XUV pulses of 10–30-ns FWHMs (When collimated p-i-n diodes were used, the pulsewidth was sometimes smaller than 3 ns). The first XUV pulses appeared at about 150 ns. The intensity of these XUV pulses was increasing with the growing time. Because the signal of the Be-filtered p-i-n diode was very small, the energy of the detected photons was mainly in the 20–70-eV region (in the transmission window of aluminum filter). For instance in Fig. 2, the energy of 20–70-eV photons emitted during the XUV pulse at about 400 ns was $\approx$ 100 mJ, whereas the energy of $>$ 1-keV photons approached 1 mJ.

1) Implosion: The only diagnostic tool, which provided images of what happened before XUV pulses, was the gated VUV pinhole camera. For example, the behavior before the first XUV pulse is displayed in Fig. 3. In this shot, during the gradual fall of dI/dt, the VUV images show the relatively stable implosion of the coronal plasma onto a fiber. The implosion velocity approached the value of $2 \cdot 10^5$ m/s. The compression ratio (i.e., the ratio of the mean maximum and minimum pinch radius) was about 10 (cf. Fig. 3). Because the compression caused the increase of the plasma inductance and resistance, we observed the voltage rise together with the drop of dI/dt.

In most cases, the implosion was nonsymmetric (most likely because of the polarity effect). As a result, the radiation was

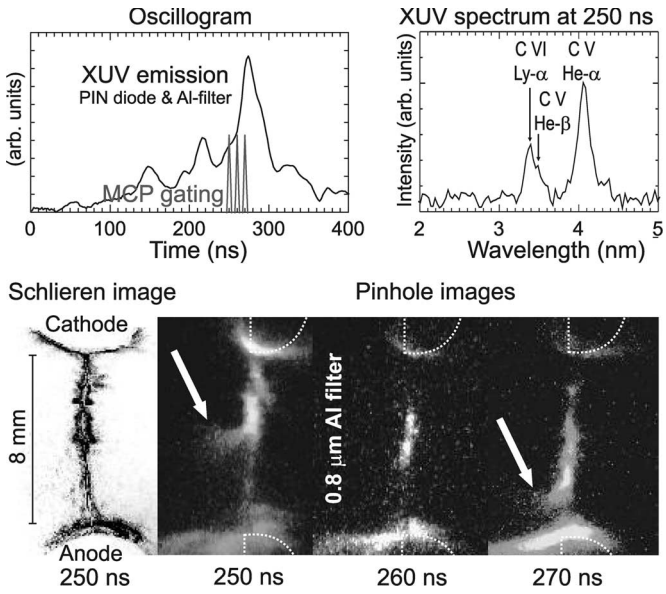

Fig. 4. Zippering from the cathode with the velocity of 10^5 m/s, shot no. 030321-1.

zippering along the fiber with the velocity of 10^5 m/s. This phenomenon could be seen in the images in Fig. 4. The zipper was spreading mainly from the cathode. At this point, we would like to point out that we have never seen the implosion in schlieren images. With regard to the pinhole camera, when an Al foil was used to filter the radiation (see pinhole image at 260 ns in Fig. 4), we observed only the zipper without any evidence of the implosion.

The plasma density during the implosion could be derived from the implosion velocity, which approached $2 \cdot 10^5$ m/s. When the kinetic pressure is small compared with the magnetic pressure, this value is of the order of the Alfvén velocity, i.e.,

$$v_{\mathrm{imp}}|_{\mathrm{MAX}} \approx 2 \cdot v_{\mathrm{Alf}} = \sqrt{\frac{\mu_0 I^2}{N_{\mathrm{i}} M_{\mathrm{i}}}}. \tag{1}$$

For the electric current $I = 40$ kA and for the mass of carbon ion $M_{\mathrm{i}} = 2 \cdot 10^{26}$ kg, we obtain the line density of ions in the coronal plasma $N_{\mathrm{i}} = 8 \cdot 10^{17}$ m^{-1}. When we take the density of carbon atoms in a fiber $n_{\mathrm{a}} = 1.1 \cdot 10^{29}$ m^{-3}, the line density of a 15-μm diameter fiber is $N_{\mathrm{a}} = 2 \cdot 10^{19}$ m^{-1}. From these values, we may conclude that roughly a few percents of the total mass of a fiber were ablated at that time.

The line density of $N_{\mathrm{i}} = 8 \cdot 10^{17}$ m^{-1} determines not only the mass of a fiber ablated but also the average plasma density. First, if we assume that the diameter of a plasma column D at the beginning of the implosion is of the order of one centimeter (cf. Fig. 3), we obtain the ion density of about $n_{\mathrm{i}} = 4N_{\mathrm{i}}/\pi D^2 = 10^{16}$ cm^{-3}. Second, at the end of the plasma implosion, we observed the plasma diameter of the order of millimeter, and hence, the ion density was about 10^{18} cm^{-3}.

The temperature measurement during the implosion was performed mainly from the lines of H- and He-like carbon ions. The He-α line was observed first during the implosion, but especially shortly before the stagnation. The evolution of Ly-α and He-α lines before the stagnation is demonstrated in Fig. 5.

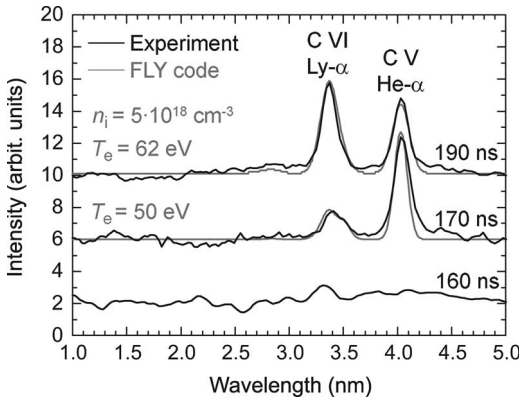

Fig. 5. XUV spectra during the implosion, shot no. 011031-3. Synthetic spectra simulated with the FLY code for optically thin plasma. The last spectrum was detected 10 ns prior to the peak of the 20-ns XUV pulse.

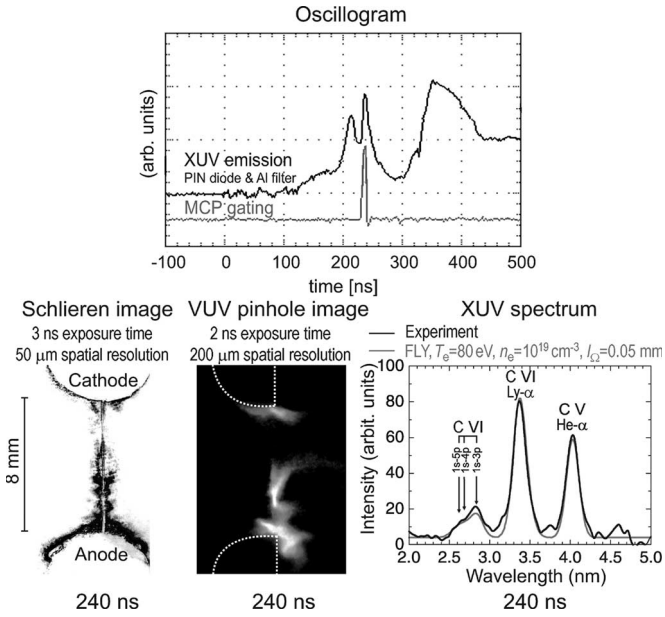

Fig. 6. Simultaneous XUV spectrum, schlieren, and pinhole images exposed at the peak of the XUV pulse, shot no. 030219-4.

If the plasma is optically thin, the Ly-α to He-α ratio is almost density independent and can serve as a convenient method for temperature measurement. Fig. 5 illustrates clearly how the Ly-α to He-α ratio was increasing during the implosion and the temperature was growing.

2) Stagnation: At the end of the implosion, a coronal plasma reached a fiber and stagnated at the axis for a brief period of time. This time corresponded to the peak of the short intensive pulse of the XUV radiation. The simultaneous diagnostics in Fig. 6 demonstrates that the radiation was emitted from that part of a fiber where the MHD instabilities were developed. These perturbations were usually axisymmetric, indicating an $m = 0$ instability. Schlieren images corresponded to pinhole images, and thus, the schlieren system and pinhole camera gave a similar value of the perturbation wavelengths. The wavelength λ and pinch radius (or to be more precise, the diameter of instabilities) R varied from 0.3 to 1 mm and 0.5 to 1.5 mm, respectively. The kR product, where $k = 2\pi/\lambda$ is the axial wavenumber, was 2–10. However, an accurate evaluation was impossible, since only a few lobes developed along the fiber.

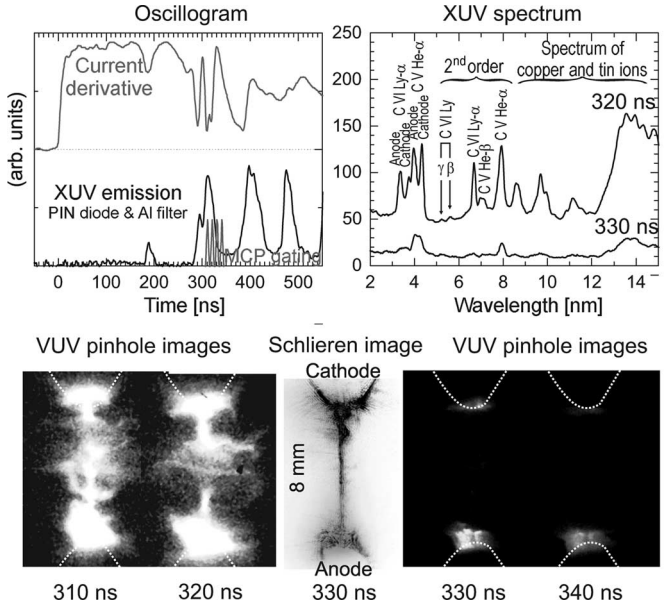

Fig. 7. Cooling after the stagnation in discharge no. 040225-2, schlieren sensitivity $n_e \approx 10^{19}$ cm^{-3}.

Fig. 6 also shows the experimental and simulated spectrum. The simulated spectrum was calculated by the collisional-radiative code FLY [18]. As far as the input parameters for the steady-state simulation are concerned, the electron temperature T_e and density n_e were 80 eV and 10^{19} cm^{-3}, respectively. Optical depth effects were taken into account. The estimation of the electron density n_e was ambiguous, owing to its dependence on the choice of the optical path length. Therefore, the plasma density was obtained from the schlieren images, assuming a parabolic density profile. On the basis of our measurements with different stops in the focus, we assumed that the average electron density during the stagnation was of the order of $n_e \approx 10^{19}$ cm^{-3}. For the average ion charge of 5, we get the ion density of $n_i \approx 2 \cdot 10^{18}$ cm^{-3}, which is two times higher than the density estimated from the implosion velocity. It is a reasonable agreement, especially if we consider that both methods give only a rough estimation, and that the density during the stagnation could be increased by the particles ablated from a fiber.

At this point, we should remark that the ion line density of about 10^{18} m^{-1} and the spectroscopically measured temperature of 80 eV together with the ionization state of 5 (He-like carbon) agree with the Bennett equilibrium for the current of 40 kA.

3) Expansion: The stagnation lasted from a several nanoseconds to a few tens of nanoseconds. After the stagnation, we observed the expansion of a plasma column (see Fig. 7, the density of a plasma column was below the sensitivity of the schlieren system already 20 ns after the peak of the XUV radiation). Determining the expansion velocity was somewhat problematic, because of the drop of the plasma density and emitted power. However, it was clear that the expansion velocity was high enough to cause the rapid increase of dI/dt. The expansion was accompanied by the gradual cooling. In Fig. 7,

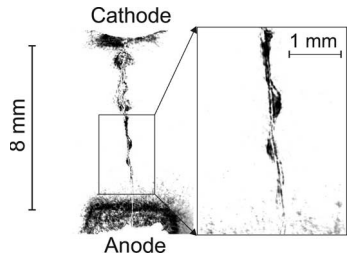

Fig. 8. Schlieren image of the helix observed at 300 ns, it occurred 50 ns after the peak of the XUV pulse in the discharge no. 030410-2.

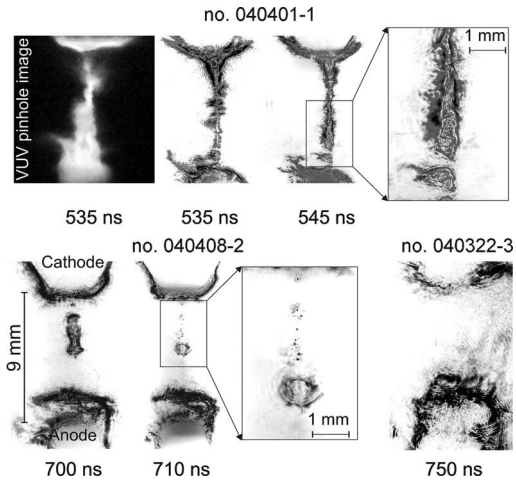

Fig. 9. Schlieren images and one pinhole image that recorded the ablation of a fiber.

the Ly-α to He-α ratio fell down during 10 ns. It means that the temperature dropped from 60 eV to less than 45 eV.

Several times, we also observed the helix after the expansion. For instance, Fig. 8 was recorded 50 ns after the XUV pulse. At this time, the plasma was expanded to a radius of several millimeters, whereas the diameter of helix was about 50 μm.

4) Multiple Pulses: Fig. 2 shows a high number of pulses that were detected by a p-i-n diode. It was necessary to decide whether pulses originated from various places along a fiber or from the whole length of a fiber at different moments.

We believe that both phenomena might occur. During the rise of the current, we observed that the multiple implosion of the corona onto a fiber took place. However, when there were more than three pulses, they did not originate from the whole length of a fiber. Especially in the case of conical electrodes, the nonsymmetric implosion occurred separately at the anode, at the cathode, and at the center.

D. Fiber Ablation and Evaporation

Approximately 500 ns after the breakdown, the melting of a carbon fiber was seen (see Fig. 9, shot no. 040401-1). Gaps in the fiber indicated that several parts of a fiber had been already ablated, especially the part near the anode. In Fig. 9, one can further see the $m = 0$ behavior, which most likely increased the ablation rate. In the case of the conical electrodes, the central part of a fiber persisted up to 700 ns and then formed a column

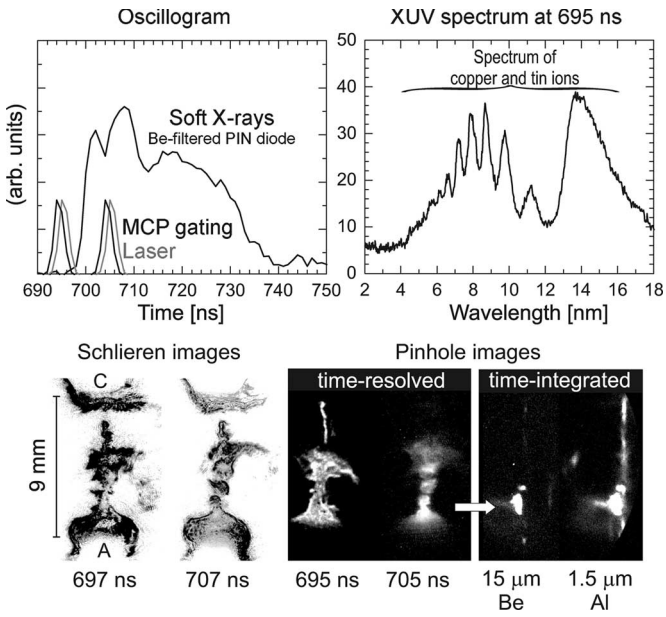

Fig. 10. Z-pinch plasma during the onset of an intensive X-ray pulse, shot no. 040414-3.

of several separated droplets less than 10 μm in diameter. The entire length of a fiber was seen totally ablated 750 ns after the current breakdown.

E. Discharge in Electrode Vapor

XUV pulses with various FWHMs were emitted also between 400 and 1000 ns. In this phase, pulses were accompanied with rises of voltage up to 30 kV (similarly to plasma-on-fiber phase). However, in comparison with the first 400 ns of the discharge, these pulses were more energetic. The energy of $>$ 1-keV photons exceeded 10 mJ in one pulse, and the abundance of $>$ 6-keV photons was detected behind a 100-μm-thick Al filter.

X-ray pulses were observed at the end of the off-axis implosion of the plasma near the anode. The implosion velocity was about $3 \cdot 10^4$ m/s. Schlieren images indicated that more mass (electron line density above 10^{20} m^{-1}) participated in the implosion than in the plasma-on-fiber phase. Since we observed that the spectral lines of higher-Z ions started to dominate in XUV spectra after 500 ns, it was evident that the important role was played by the material of electrodes (see Fig. 10, one may also notice the peak of tin ions at 13.5 nm, which has become important for the EUV lithography).

The final stage of the implosion was detected in shot no. 040414-3 (see Fig. 10). In this particular shot, images were obtained just before and during the X-ray pulse of a 2-ns rise time. The schlieren and pinhole images caught the development of the $m = 0$ instability with three blobs. Furthermore, the most intensive radiation (as could be seen in the time-integrated pinhole images) came from one off-axis elongated bright spot, which corresponded to the constriction of one $m = 0$ neck. These bright spots occurred mainly near the anode, and their number was shot-to-shot dependent. Since spectral lines of Cu XIX ions (e.g., $3d\ ^2D - 4f\ ^2F$ transition at 4.74 nm) were

identified in the XUV spectra, the electron temperature was above 100 eV.

At this point, we shall turn to the plasma-on-fiber stage. In Fig. 10, the entire length of a carbon fiber is displayed in the time-integrated Al-filtered pinhole image. The radiation from a fiber was absorbed by the Be-filter. Such result agrees with the observation of the XUV pulses (and no X-ray pulses) during the plasma-on-fiber phase. Next, the spatially nonuniform exposure along the fiber gave another evidence that the radiation came from that part of a fiber where an $m = 0$ instability developed.

F. Z-Pinch Disintegration

The disintegration of the Z-pinch occurred at about 1 μs. At that time, discharge chamber walls were most likely reached by the ejecta of a plasma. Also, X-ray and UV flux emitted from a Z-pinch could envelop the surface of the insulator with a plasma. Due to that, the significant part of the current was flowing outside the Z-pinch region and the decreasing amount of radiation was detected.

G. Z-Pinch Energetics

The measurement of the plasma voltage and the current together with sequences of images and spectra enabled us to estimate the energy deposited into our Z-pinch. We found that during the implosion, the energy was coupled from the generator through a time-varying inductance. The electrical energy was mainly converted 1) into the radial motion of ions; 2) into the (adiabatic) compression of a plasma column; and 3) into the increase of magnetic energy. However, the global implosion of a plasma column formed only a fraction (typically 1/5) of the total energy delivered into a plasma during one XUV pulse. Moreover, the global implosion cannot fully explain the measured value of the $R_{\rm P} + dL_{\rm P}/dt$ term (up to 0.3 Ω).

Late in the implosion, as the radius R and velocity $v_{\rm imp}$ were decreasing, the influence of the plasma resistance was growing, and the resistive heating started to play an important role. The substantial contribution to the plasma-column resistance during the stagnation could be ascribed to instabilities. The strong argument for that are the voltage spikes, which corresponded to the XUV pulses. At the same time, these XUV pulses did not originate from the whole length of a fiber but from several bright spots (see Fig. 10). These bright spots corresponded to the interaction of the necks of an $m = 0$ instability with the dense core. Nevertheless, despite the fact that we took into account that $m = 0$ instabilities contributed not only to the plasma resistance but also to the $dL_{\rm P}/dt$ term, it was still not satisfactory to explain the $R_{\rm P} + dL_{\rm P}/dt$ value with the Spitzer resistivity and with the radius of $m = 0$ instabilities > 100 μm. One of possible explanations of this discrepancy might be an anomalous resistivity rather than a smaller radius of instabilities. Another possible, however less probable explanation might be a sudden onset of an $m = 1$ instability.

The total deposited energy was spent on the evaporation of a fiber and electrodes, ionization and heating of a plasma, thermal diffusion, advection, etc. Only a small part of the energy was radiated from the plasma. Some of the important parameters of our Z-pinch are summarized in Table I.

TABLE I
ENERGETICS OF OUR FIBER Z-PINCH

Physical quantity	Energy
Energy stored in a capacitor bank $\frac{1}{2}C_0U_0^2$	600 J
Energy deposited into a plasma $\int_0^\infty (U_{\rm P} - L_{\rm P}\dot{I})I dt$	$\approx$ 100 J
Implosion energy deposited into a plasma	$\approx$ 20 J
Emitted energy	$\approx$ 5 J
Energy emitted in the XUV region (20–70 eV)	$\approx$ 300 mJ
Energy emitted in soft X–rays ($>$ 1 keV)	$\approx$ 20 mJ

IV. DISCUSSION

In the discussion that follows, we shall first summarize the most important results of other fiber experiments. Then, we will point out results, which are similar or different to ours. The particularity of our fiber Z-pinch is the implosion of a coronal plasma onto a fiber, and thus, it will be treated of in more detail. Finally, we will deal with bright spots observed in our discharge.

A. Fiber Z-Pinch Experiments

Fiber Z-pinch experiments were carried out on modern high-voltage pulsed-power generators at Los Alamos National Laboratory [1], [4], [6], [7], Naval Research Laboratory [2], [19], Imperial College in London [8]–[13], Kernforschungszentrum Karlsruhe [5], and Kurchatov Institute in Moscow [20]. Even though each experimental group observed somewhat a different behavior of a fiber Z-pinch, the gross dynamics of a fiber pinch was described. We shall sum up the most important findings of these research groups in the following text.

We start with the global expansion of a coronal plasma surrounding the solid core. The expansion was observed, although the Pease-Braginskii current was reached and the current rise was fast enough to cause the radiative collapse. This rapid expansion could happen for several reasons, and we touch upon them briefly. One of the reasons might be the anomalous resistivity in a low-density coronal plasma, which, if it occurs, causes the plasma kinetic pressure to exceed the magnetic pressure [21]. As a result, the Bennett equilibrium does not hold and the pinch expands. Another reason for the expansion may lie in the MHD instabilities. During the development of an $m = 0$ instability, the bulges of the instability expand and the constricted regions cause the enhanced nonuniform heating of the core [6], [7]. As for $m = 0$ instability, it was apparent very early in the discharge in shadowgrams and schlieren images. These instabilities exhibited a highly dynamic behavior [8], but they were not disruptive (most likely because of the dense core, which lasted for a relative long time). During the interaction of the coronal plasma with the remaining dense core, the bright spots occurred. After the dynamic bright-spot phase, the disruption accompanied with the neutron production, and the X-ray emission was observed as soon as the fiber was completely ablated [2], [3].

All these results, but mainly the rapid expansion and the early development of plasma instabilities, effectively decrease

the plasma density and eliminate the possibility of using a fiber Z-pinch as a fusion reactor.

B. Implosion of Coronal Plasma Onto Central Fiber

Our work with a carbon-fiber Z-pinch brought some results that were to a certain extent similar to those of the aforementioned experiments, despite the fact that the peak currents and the rise times were substantially different. Similarly to these experiments, we made the following observations.

1) A low-density coronal plasma carried almost all the current, a cold dense core persisted for a long time. The interaction of a coronal plasma with this dense core then substantially influenced the plasma dynamics.
2) The XUV emission came mainly from the bright spots, which were produced by the instabilities that developed in a low-density corona. However, these instabilities were not disruptive as long as the dense core survived unionized.
3) After the fiber ablation, the intense X-ray radiation was produced.

Nevertheless, our Z-pinch differed in several issues of a great importance too. Fiber Z-pinches, which are driven by the fast pulsed power generators, are usually considered to be in pressure balance, because the current rises rapidly and the plasma pressure could be balanced against the magnetic forces in every moment. Contrary to that, our fiber Z-pinch, which was driven by a microsecond capacitive discharge, expanded first to the diameter of about 1 cm. When the current built up, the implosion of a coronal plasma onto a central fiber occurred. This means that our fiber Z-pinch behaved as a dynamic pinch for a lapse of time. Even though the current was about 40 kA, the implosion velocity approached the value of $2 \cdot 10^5$ m $\cdot$ s^{-1}.

It is true that a noticeable implosion could be observed also on the pulsed power generators; however, the current prepulse must be applied. Such experiment was carried out by Lorenz *et al.* on the IMP generator ($I_{\max} = 200$ kA, $t_{10\%-90\%} = 60$ ns, IC London, [10]). In this experiment, the prepulse delivered a 10-kA current with a 50-ns quarter period into a 7-μm diameter carbon fiber. The breakdown of the fiber occurred when the voltage reached about 20 kV. The prepulse generated a low-density coronal plasma of $N_{\rm i} = 3 \cdot 10^{17}$ m^{-1} (cf. with our value of $8 \cdot 10^{17}$ m^{-1}), which expanded to a radius of the order of a millimeter. After the switch of the main discharge current, they observed similarly as we did, the implosion of a low-density plasma onto a fiber (In Lorenz's experiment, the faster current rise time implied a lower skin depth), the zipper from the cathode toward the anode, the soft X-ray pulse, and subsequent rapid expansion.

Another similar feature between Lorenz's and our experiment was the observation of $m = 0$ and $m = 1$ instabilities during the stagnation of the corona at the fiber. Despite a low Lundquist number (during the stagnation $S \approx 10$), the enhanced stability was not confirmed, and the presence of a fiber did not seem to significantly suppress the MHD instabilities. However, these were not excessively disruptive. With regard to $m = 1$ instabilities, they were observed in the pinhole images, whereas in the schlieren images, they were less apparent. The complex helical structures developed usually during an expansion phase after the stagnation (see Fig. 8 and [22]). Recently, the influence of an $m = 1$ instability upon the Z-pinch dynamics has been quantitatively discussed in [23].

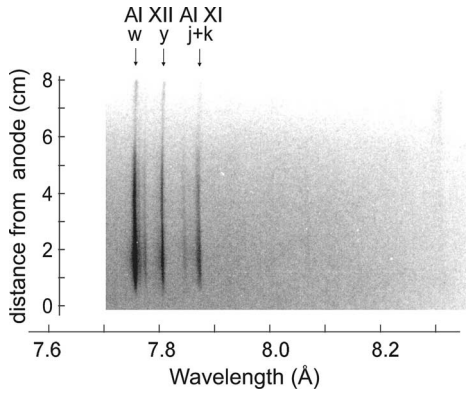

Fig. 11. Spatially resolved X-ray spectrum recorded during the implosion of the deuterium plasma sheath onto an Al wire (80-μm diameter and 8-cm length), PF-1000 plasma focus (IPPLM, Warsaw), shot no. 2565, 1.5-MA peak current, deuterium filled up to 3 Torr.

In our and Lorenz's experiments, the coronal plasma was formed from a fiber. Another possibility would be to create a plasma from a wire array or gas puff, which subsequently implodes onto a central fiber. These two approaches were tried on the Z-machine [24] and on the S-300 generator [25]. In the latter experiment, the implosion of a wire array had the positive influence on the neutron yield. The neutron yield was one order in magnitude higher in the case of an imploding wire array onto a fiber than without a wire array [20].

With regard to the difference between the coronal plasma created from a fiber and the plasma formed from a wire array or a gas puff, the higher mass was imploded onto a fiber in experiments with the wire arrays or gas puffs. Clearly, the energetics of these Z-pinches is dominated by the implosion energy. In our fiber experiment, the implosion energy was relatively low. Much more important phenomenon was probably the transfer of the current in the vicinity of a fiber when the corona imploded.

C. Plasma on Wire

The peculiarity of a solid fiber is its initial nonconductivity that causes the transfer of the current from a fiber, and thus makes the energy coupling into a fiber difficult. Different situation occurs when a conducting wire is used instead of a fiber. The implosion of an aluminum jet onto a coaxial aluminum wire was first studied in [26]. Wessel *et al.* found the resultant plasma to be more uniform and hotter than a wire-only and jet-only pinch. The pinch also demonstrated that an imploding plasma could couple the energy from a current generator to a micrometer-sized wire.

The experiments on the PF-1000 plasma focus in Warsaw showed a similar behavior [27]. In some shots with a deuterium filling, an Al wire was placed at the axis and top of the anode, having no galvanic connection to the anode. Fig. 11 shows the spatially resolved spectrum recorded with the time-integrated X-ray spectrograph, which detected resonance,

intercombination, and satellite lines of He-like aluminum ions. Clearly, the whole length of an Al wire did not manifest typical large-scale instabilities, which are the characteristics for wire Z-pinches. If we realize that the length of a wire was 8 cm, it was quite an impressive result for a pinch plasma, which may lead to reconsideration of a wire Z-pinch as an X-ray laser medium.

D. Bright Spots

In our experiment, we have to distinguish two types of bright spots. The first group of bright spots was produced during the plasma-on-fiber phase. These bright spots emitted less energetic photons than bright spots created in the electrode vapor. The X-ray photons were generated from the latter bright spots for several reasons. First, instabilities could develop substantially after the fiber had been already ablated. Second, the current at this phase was higher than in the plasma-on-fiber stage. Third, the plasma contained ions (Cu, Sn, etc.) with higher atomic number Z than a carbon has. As a result, radiation losses were increased and $m = 0$ instabilities could develop according to the radiative collapse model. As far as the position of the bright spots occurrence is concerned, they appeared at random times and at random places but predominantly near the anode, similarly to vacuum sparks [28].

V. Conclusion

In conclusion, it should be stressed that the dynamics of a fiber Z-pinch substantially differs from Z-pinches initiated from a metal wire. Even though the ICF purposes caused a carbon-fiber Z-pinch to be of a modest interest now, we believe that the unique properties of a carbon could provide valuable data not only for Z-pinch physics but also for life science (carbon K-shell lines are in the water window) and material science, in which a carbon is often used. Our experiment with a carbon fiber proved that it is possible to study a lot of Z-pinch phenomena on a small device, provided that a plasma is thoroughly diagnosed. As an example, we could mention the study of the Z-pinch implosion with the velocity above 10^5 m/s on the current level of 50 kA. Another interesting phenomenon is the implosion onto a fiber or wire. First, it offers a possibility of transferring the current with a sharp rise-time in the vicinity of a fiber. It also provides an opportunity for modifying shape of an X-ray pulse. Next, the fiber in the center of an imploding plasma introduces homogeneity to Z-pinch discharges. Last but not least, a fiber can be used as a target for an imploding plasma and can serve as a diagnostic tool.

Our results also showed that dynamics of a fiber Z-pinch significantly varies depending on a current generator used. The current waveform of a low-impedance and low-voltage capacitor is quite sensitive to the Z-pinch behavior, especially to the change of the $R_{\mathrm{P}} + dL_{\mathrm{P}}/dt$ term. Although this fact is considered to be a disadvantage, it can serve well some diagnostic purposes (e.g., a rough estimation of the diameter of a plasma column, in which the current is flowing). Further, the voltage and the current can be quite easily measured on a low-voltage generator, and thus, we can calculate a plasma resistance and energetics of a Z-pinch.

Acknowledgment

The authors would like to thank Dr. V. Romanova (P.N. Lebedev Physical Institute, Moscow) and the research team at Institute of Plasma Physics and Laser Microfusion, Warsaw for graciously allowing them to use the data from the PF-1000 plasma focus.

References

[1] D. Scudder, "Experiments on high-density Z-pinches formed from solid deuterium fibers," *Bull. Amer. Phys. Soc.*, vol. 30, p. 1408, 1985.

[2] J. Sethian, A. Robson, K. Gerber, and A. DeSilva, "Enhanced stability and neutron production in a dense Z-pinch plasma formed from a frozen deuterium fiber," *Phys. Rev. Lett.*, vol. 59, no. 8, pp. 892–899, Aug. 1987.

[3] I. Lindemuth, "Two-dimensional fiber ablation in the solid-deuterium Z-pinch," *Phys. Rev. Lett.*, vol. 65, no. 2, pp. 179–182, Jul. 1990.

[4] J. Shlachter, "Solid D2 fiber experiments on HDZP-II," *Plasma Phys. Control. Fusion*, vol. 32, no. 11, pp. 1073–1081, 1990.

[5] W. Kies, G. Decker, M. Malzig *et al.*, "Terawatt fiber pinch experiments," *J. Appl. Phys.*, vol. 70, no. 12, pp. 7261–7272, Dec. 1991.

[6] P. Sheehey, J. Hammel, I. Lindemuth *et al.*, "Two-dimensional direct simulation of deuterium fiber initiated Z-pinch with detailed comparison to experiment," *Phys. Fluids B*, vol. 4, no. 11, pp. 3698–3706, Nov. 1992.

[7] R. Riley, D. Scudder, J. Shlachter, and R. Lovberg, "Instability heating of a solid fiber Z-pinch," *Phys. Plasmas*, vol. 3, no. 4, pp. 1314–1323, Apr. 1996.

[8] J. Chittenden, I. Mitchell, R. Aliaga-Rossel *et al.*, "The dynamics of bifurcation bright-spots in fiber Z-pinch plasmas," *Phys. Plasmas*, vol. 4, no. 8, pp. 2966–2967, Aug. 1997.

[9] F. Beg, A. Dangor, P. Lee, M. Tatarakis, S. Niffikeer, and M. Haines, "Optical and X-ray observations of carbon and aluminium fibre Z-pinch plasmas," *Plasma Phys. Control. Fusion*, vol. 39, no. 1, pp. 1–25, 1997.

[10] A. Lorenz, F. Beg, J. Ruiz-Camacho, J. Worley, and A. Dangor, "Influence of a prepulse current on a fiber Z-pinch," *Phys. Rev. Lett.*, vol. 81, no. 2, pp. 361–364, Jul. 1998.

[11] S. Lebedev, R. Aliaga-Rossel, J. Chittenden *et al.*, "Coronal plasma behavior of the Z-pinch produced from carbon and cryogenic deuterium fibers," *Phys. Plasmas*, vol. 5, no. 9, pp. 3366–3372, Sep. 1998.

[12] I. Mitchell, R. Aliaga-Rossel, J. Chittenden, A. Robledo, H. Schmidt, and M. Haines, "Investigation of electron and ion beams in mega-ampere fiber pinch plasmas," *IEEE Trans. Plasma Sci.*, vol. 26, no. 4, pp. 1267–1273, Aug. 1998.

[13] M. Haines, S. Lebedev, J. Chittenden, F. Beg, S. Bland, and A. Dangor, "The past, present, and future of Z pinches," *Phys. Plasmas*, vol. 7, no. 5, pp. 1672–1680, May 2000.

[14] I. Mitchell, J. Bayley, and J. Chittenden, "A high impedance megaampere generator for fiber Z-pinch experiments," *Rev. Sci. Instrum.*, vol. 67, no. 4, pp. 1533–1541, Apr. 1996.

[15] P. Kubes and J. Kravarik, "Carbon fiber X-ray lasing," in *Proc. 4th Int. Conf. Dense Z-Pinches, AIP Conf.*, New York, 1997, pp. 449–453.

[16] J. Haun, H. Kunze, S. Kosse, M. Schlanges, and R. Redmer, "Electrical conductivity of nonideal carbon and zinc plasmas: Experimental and theoretical results," *Phys. Rev. E, Stat. Phys. Plasmas Fluids Relat. Interdiscip. Top.*, vol. 65, no. 4, p. 046407, Apr. 2002.

[17] G. Sarkisov, P. Sasorov, K. Struve *et al.*, "Polarity effect for exploding wires in a vacuum," *Phys. Rev. E, Stat. Phys. Plasmas Fluids Relat. Interdiscip. Top.*, vol. 66, no. 4, p. 046413, Oct. 2002.

[18] R. Lee, "A time-dependent model for plasma spectroscopy of K-shell emitters," *J. Quant. Spectrosc. Radiat. Transfer*, vol. 56, no. 4, pp. 535–566, Oct. 1996.

[19] F. Young, S. Stephanakis, and D. Mosher, "Neutron and energetic ion production in exploded polyethylene fibers," *J. Appl. Phys.*, vol. 48, no. 9, pp. 3642–3650, Sep. 1977.

[20] D. Klir, P. Kubes, J. Kravarik *et al.*, "Deuterated fibre Z-pinch on S-300 generator," *Phys. Scripta*, vol. T123, pp. 116–119, Mar. 2006.

[21] J. Chittenden, , "The effect of lower hybrid instabilities on plasma confinement in fiber Z-pinches," *Phys. Plasmas*, vol. 2, no. 4, pp. 1242–1249, Apr. 1995.

[22] R. Spielman, J. DeGroot, and T. Nash, "Stagnation dynamics and heating mechanisms for wire array Z-pinch implosions," in *Proc. 3th Int. Conf. Dense Z-Pinches, AIP Conf.*, New York, 1997, pp. 404–420.

[23] J. Chittenden, S. Lebedev, C. Jennings, S. Bland, and A. Ciardi, "X-ray generation mechanisms in three-dimensional simulations of wire array Z-pinches," *Plasma Phys. Control. Fusion*, vol. 46, no. 12B, pp. B457–B476, Dec. 2004.

[24] R. Spielman, G. Baldwin, G. Cooper *et al.*, "D-D fusion experiments using fast Z pinches," Sandia Nat. Lab., Albuquerque, NM, Rep. SAND98-07-05, 1998.

[25] D. Klir, P. Kubes, J. Kravarik *et al.*, "Wire-array implosion onto a deuterated fibre at the S-300 facility," *Plasma Devices Oper.*, vol. 13, no. 1, pp. 39–43, Mar. 2005.

[26] F. Wessel, B. Etlicher, and P. Choi, "Implosion of an aluminium plasma-jet onto a coaxial wire: A Z-pinch with enhanced stability and energy transfer," *Phys. Rev. Lett.*, vol. 69, no. 22, pp. 3181–3184, Nov. 1992.

[27] L. Karpinski, J. Kravarik, P. Kubes *et al.*, "Soft X-ray spectral investigation in wire-in-plasma focus experiments," *Plasma Phys. Control. Fusion*, vol. 44, no. 8, pp. 1609–1614, 2002.

[28] K. Koshelev and N. Pereira, "Plasma points and radiative collapse in vacuum sparks," *J. Appl. Phys.*, vol. 69, no. 10, pp. R21–R44, May 1991.

Daniel Klir was born in Podebrady, Czech Republic, on March 4, 1979. He received the M.Sc. degree in applied physics and the Ph.D. degree in plasma physics from the Czech Technical University (CTU), Prague, Czech Republic, in 2002 and 2005, respectively.

In 2005, he became a Research Associate with the Department of Physics, Faculty of Electrical Engineering, CTU. His research interests include X-ray spectroscopy, plasma diagnostics, and Z-pinch physics.

Pavel Kubes was born in Prague, Czech Republic, on May 23, 1943. He received the M.Sc. degree in astrophysics from Charles University, Prague, in 1965 and the Ph.D. degree in plasma physics from the Czech Technical University (CTU), Prague, in 1977.

In 1966, he joined the Department of Physics with the Faculty of Electrical Engineering, CTU. From 1990 to 2003, he was the Head of the Department of Physics. In 1991, he became an Associate Professor, and since 1998, he has been a Professor of applied physics. His research interests concentrate on the study of X-rays and neutrons in Z-pinch and plasma focus discharges at CTU Prague, Institute of Plasma Physics and Laser Microfusion (IPPLM) Warsaw and Russian Research Centre 'Kurchatov Institute' (RRC KI) Moscow.

Jozef Kravarik was born in Bosaca, Slovakia, on August 9, 1936. He received the M.Sc. degree in electrical engineering and the Ph.D. degree in plasma physics from the Czech Technical University (CTU), Prague, Czech Republic, in 1960 and 1967, respectively.

In 1963, he joined the Faculty of Electrical Engineering, CTU, as an Assistant Professor, and since 1976, he has been an Associate Professor. His research activities concentrate on the visual, X-ray, laser, and high-energy particle diagnostics of the Z-pinch and plasma focus discharges at CTU, Institute of Plasma Physics and Laser Microfusion (IPPLM) Warsaw and Russian Research Centre 'Kurchatov Institute' (RRC KI) Moscow.